Dynamics of pedestal profiles in ELMy H-mode plasmas in TCV at different collisionalities

A. Pitzschke[1], R. Behn[1], B.P. Duval[1], G. Induni[1], S. Yu. Medvedev[2], L. Porte[1], O. Sauter[1], and TCV team

[1] *École Polytechnique Fédérale de Lausanne (EPFL),*
Centre de Recherches en Physique des Plasmas, Assoc. EURATOM-Confédération Suisse,
CH-1015 Lausanne, Switzerland
[2] *Keldysh Institute of Applied Mathematics, Russian Academy of Sciences,*
Moscow, Russian Federation

The dynamics of the profiles of electron temperature, density and pressure during H-mode phases in the TCV tokamak has been investigated for cycles with ELMs of type I and type III, characterized by different regimes of collisionality ($v^\star = 10^{-14} Z_{eff} R_0 n_e T_e^{-2}$) of the plasma near the edge. Quasi-stationary H-mode phases with ELMs of type-III at $v^\star = 0.75$ were already obtained in TCV with ohmic heating only, whereas additional power from electron cyclotron heating (ECH) was necessary to reach a regime at lower collisionality ($v^\star = 0.40$) with large ELMs of type I . The main plasma parameters like current, line-averaged density and shaping were identical for both series of shots analysed in this study ($I_p : 370kA, B_T : 1.43T, q_{95} : 2.3, \overline{n_e \cdot L} : 3.2 - 3.6 \cdot 10^{19} m^{-2}, \kappa : 1.7, \delta : 0.45$) and a plasma configuration with single-null X- point and ion ($B \times \nabla B$)- drift in the favourable direction was chosen. For ECH at the 3rd harmonic, 2 gyrotrons operating at 118GHz injected a total power of 1MW launched in vertical direction from the top of the TCV vessel. The profiles were measured using the Thomson scattering system on TCV, equipped with channels of high spatial resolution to resolve the expected gradients in the so-called pedestal region. With an effective repetition rate of 60Hz set by the Nd:YAG lasers, this diagnostic does not seem suitable to follow the time evolution during ELM cycles with a period in the range of 5 to 25ms. However, in cases with extended and quasi-stationary H-mode phases and for series of reproducible shots, the method of random sampling and coherent averaging can be used to reconstruct a typical ELM cycle with an effective time resolution on the ms scale. For this analysis, the profiles measured on a vertical chord were projected onto flux surfaces and then onto radial coordinates in the equatorial plane. After fitting by an analytical function (*tanh*) the profiles were characterised by a set of parameters to describe their time evolution [1]. Other diagnostics, like ECE and Lithium ion beams, have been used to measure edge profiles [2]. A major advantage of using Thomson scattering relies in the fact that electron temperature and density are obtained simultaneously and at the same locations. Therefore, this technique has also been applied on other machines [3].

Profile evolution during the ELM cycle

The results for the case of type-III ELMs with $v^\star = 0.75$ at the pedestal are shown in fig. 1. Although the analysis is based on many ELM events within a series of shots, due to good reproducibility within the selected time windows, the major tendencies are clearly revealed. A complication arises from the fact that in these shots the central value of the safety factor was close to one and sawtooth activity is observed also during the ELMy H-mode phases. Although the sawtooth period is shorter (by a factor of 2 to 3) than the ELM period, some signs of a correlation between sawtooth and ELM events are seen (frame vi of fig. 1). During the pre-ELM phase, no significant variation of the profile parameters is observed, apart from a sudden rise in the gradients during an interval of 1 to 2ms before the ELM event (identified as the maximum of the spike in the D_α emission). This seems to be correlated with the maximum probability for a sawtooth event, which may play the role of an ELM trigger. At the time of the ELM, a rapid

collapse of the pedestal heights for temperature and density profiles occurs; at the same time the edge gradient in the density and pressure profiles flatten. Central temperature and density are not affected by the ELMs; their variation during the cycle can be attributed to correlated sawtooth activity. Recovery of the profile parameters to their pre-ELM values is accomplished after 5 to 8ms, i.e. after about half of the ELM period.

The same procedure has been applied to analyze the cases with ELMs of type I under conditions of additional ECH and the results are shown in fig. 2. The temperatures at the edge pedestal are significantly higher (500eV instead of 300eV) and $T_{e,ped}$ as well as ∇T_e rise monotonically during the pre-ELM phase. Again, the ELM event provokes a sudden drop of $T_{e,ped}$ and ∇T_e. The evolution of the density profiles is similar, but there is no increase of pedestal
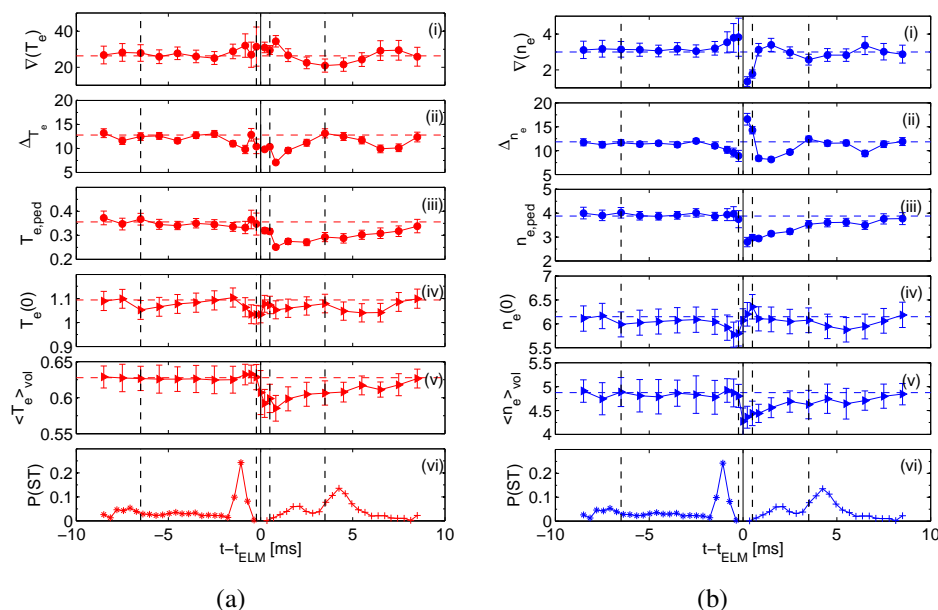
Figure 1: Time evolution of profile parameters during cycles with type-III ELMs
(a) temperature, (b) density, (i) max. gradient, (ii) pedestal width, (iii) pedestal height,
(iv) centre value, (v) vol.-averaged value, (vi) probability for sawtooth event
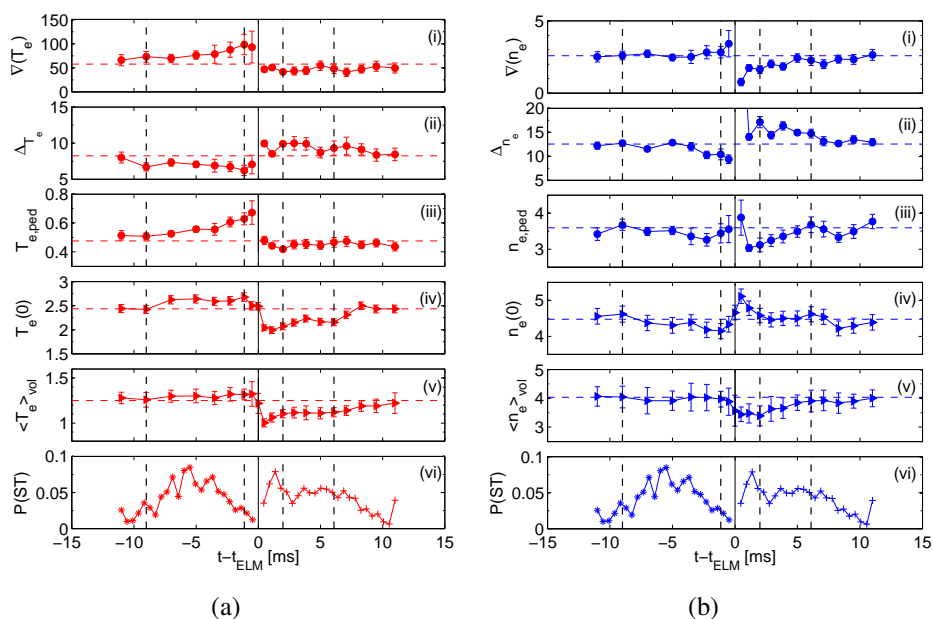
Figure 2: Time evolution of profile parameters during cycles with type-I ELMs
same identification as in fig. 1

height nor max. gradient during the pre-ELM phase. Rather, the central $n_e(0)$ decreases slightly while $T_e(0)$ rises, which is interpreted as a consequence of pump-out due to central ECH. The decrease in $n_{e,ped}$ and even $\langle ne \rangle_{vol}$ due to the ELM are indicative of a significant loss of particles from the plasma. The re-build of the profiles after the ELM event seems to be slightly faster for the density than for the temperature profiles, with time constants varying from about $1/4$ to $1/2$ of the ELM period.

(a)   (b)

(c)   (d)
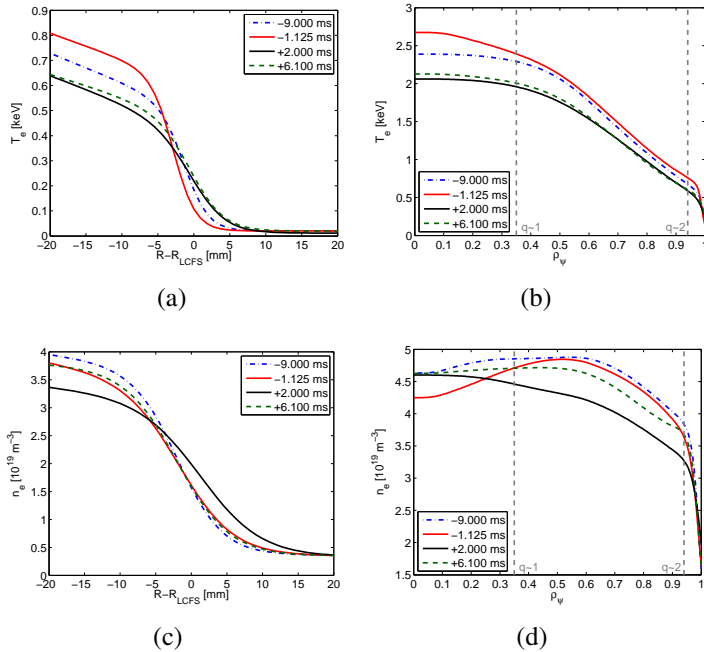
Figure 3: Profiles of T_e and n_e at selected times during a cycle with type-I ELMs

Additional insight into the time evolution is gained from the representations of the fitted profiles shown in fig. 3, both for the pedestal region and the full normalized radius. In case of the large type-I ELMs obtained by ECH, the collapse of the temperature affects the full profile up to the centre, which explains the rather high relative energy loss per ELM of 36% for the electron population (20% according to global measurements by a diamagnetic loop). Analysis of the soft X-ray emissivity have shown that there is no measurable delay between the crash seen near the edge and in the centre, which excludes the implication of diffusive processes. Further investigations and simulations are necessary to clarify whether there is an interaction of MHD modes located near the edge and in the core, respectively.

From this analysis, we also found indications for a periodic displacement of the region of maximum gradient relative to the separatrix. The effect is more pronounced in the case of type-I ELMs and may be described as an inward displacement during the pre-ELM phase, followed by fast motion in the opposite direction after the ELM event (see fig. 4, displacement normalized to pedestal width, scale relative to separatrix location R_{LCFS}). The experimental data presented here provide strong constraints on transport models describing the ELM collapse. Preliminary results from a 1 1/2-D transport code (ASTRA) have shown that a simple increase of the local heat diffusivity is not sufficient to reproduce this complex behaviour.

Figure 4: Displacement of edge barrier with respect to separatrix for type-I ELMs

Stability limits according to ideal MHD

On the basis of the measured pressure profiles, the stability of the plasma edge against ballooning and coupled kink-ballooning modes was investigated using KINX [4]. Since during

this study, the CXRS diagnostic on TCV could not yet provide ion temperature and density profiles with sufficient temporal and spatial resolution, the total pressure profiles were obtained by scaling of the electron component. However, the assumption of $T_e = T_i$ at the pedestal shoulder has been confirmed by time-averaged CXRS measurements. As opposed to cases presented earlier for type-III ELMs [1], the resistivities at $\nu^\star = 0.75$ and in particular at $\nu^\star = 0.40$ are sufficiently low to apply ideal MHD. Fig. 5 shows stability diagrams in the parameter space of normalized pressure gradient and normalized parallel current density near the edge. The edge current density is dominated by the bootstrap current component, which was calculated from the density and temperature profiles using [5]. The diagrams reveal the stability limits set by the pressure-driven high-n ballooning modes (solid red line) and the kink-ballooning modes at intermediate and low n, which become important with increasing edge current density. The points marked by square symbols and labelled A, B, C, and D refer to specific conditions during the ELM cycle (A : time-average over the ELM cycle, B : -5ms before ELM, C : -1.5ms before ELM, D : +1.5ms after ELM). In the case of ELMs at higher $\nu^\star$, the operational point C is close

(a)   (b)   (c)
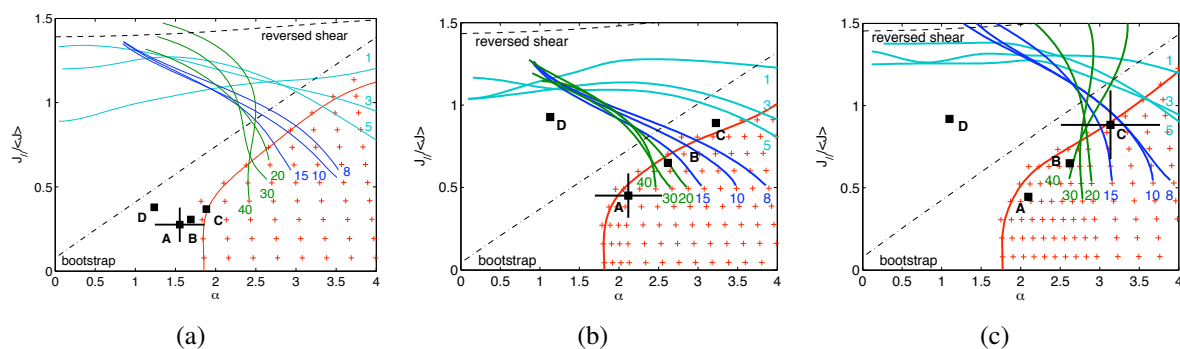
Figure 5: Stability diagram for the plasma edge from ideal MHD calculations
Referring to : (a) type-III ELMs, (b) and (c) type-I ELMs.
Stability limits : (red) high-n ballooning modes, (green, blue) kink-ballooning modes

to the limit for high-n ballooning modes (Fig.5(a)). The excursions in $J - \alpha$ parameter space during an ELM cycle remain small, leading to a shorter ELM period. Proximity to a stability limit seems to be a necessary condition, but a clear threshold effect could not be identified. For the type-I ELMs in EC-heated TCV plasmas, the analysis needs to take into account the displacement of the gradient region with respect to the separatrix. Fig. 5(b) refers to a location of the maxima for p' and bootstrap current at $\rho_0 = 0.99$ whereas Fig. 5(c) has been obtained using $\rho_0 = 0.98$, i.e. an inward shift in agreement with the experimental data (point C). In this case, access to the 2nd stability region permits higher max. pressure gradients and the stability limits are set by medium-n kink-ballooning modes. These modes have wider radial extent than those responsible for the type-III ELMs, which partially explains the higher energy and particle losses.

References

[1] Behn R *et al* 2007 *Plasma Phys. Control. Fusion* **49** 1289

[2] Wolfrum E *et al* 2009 *Plasma Phys. Control. Fusion* **51** 124057

[3] Beurskens M N A *et al* 2009 *Nucl. Fusion* **49** 125006

[4] Degtyarev L *et al* 1997 *Comput. Phys. Comm.* **103** 10

[5] Sauter O *et al* 1999 *Phys. of Plasmas* **6** 2834